Dynamic stabilization of Janus sphere *trans*-dimers

Joel N. Johnson,[1] Amir Nourhani,[1,2,3,*] Robert Peralta,[1] Christopher McDonald,[1] Benjamin Thiesing,[1] Christopher J. Mann,[1] Paul E. Lammert,[2,3] and John G. Gibbs[1,†]

[1]*Department of Physics and Astronomy, Northern Arizona University, Flagstaff, Arizona 86011, USA*

[2]*Center for Nanoscale Science, Pennsylvania State University, University Park, Pennsylvania 16802, USA*

[3]*Department of Physics, Pennsylvania State University, University Park, Pennsylvania 16802, USA*

(Received 25 January 2017; revised manuscript received 8 March 2017; published 25 April 2017)

We experimentally investigated the self-assembly of chemically active colloidal Janus spheres into dimers. The *trans*-dimer conformation, in which the two active sites are oriented roughly in opposite directions and the particles are osculated at their equators, becomes dominant as the hydrogen peroxide fuel concentration increases. Our observations suggest high spinning frequency combined with little translational motion is at least partially responsible for the stabilization of the *trans*-dimer as activity increases.

DOI: 10.1103/PhysRevE.95.042609

I. INTRODUCTION

Autonomous active colloids harvest fuel from their environment and transduce chemical energy into motion [1–4]. In comparison to passive colloids, the motility and surface activity of colloidal nanomotors and microswimmers lead to new emergent phenomena such as activity-induced clustering [5,6], motility-induced phase separation [7–10], chiral diffusion [11], spiral diffusion [12–14], autonomous microdrilling [15], passive alignment [16] and schooling behavior [17,18]. Among the goals of the field is utilizing active colloids and their emergent phenomena for simulating biological species [19] at the microscale, developing active drug-delivery vehicles [20] and constructing task-specific nanomachines [21].

Active colloids have rich dynamics and are potentially the precursors to such functional nanomachines. In order to exploit these active particles in the development of relevant exciting technologies, increasing our understanding of particle-particle interactions, self-assembly and collective dynamics of active colloids is vital. Janus microswimmers [22–25], which are spherical particles with two hemispheres of distinct surface composition (see Fig. 1), serve as standard particles for studying the dynamics of active colloids. Upon moving and interacting, Janus spheres may self-assemble into clusters of various sizes [26]. Here, however, we focus on the intriguing behavior of dimers.

Previously, Ebbens *et al.* [25] investigated deterministic and stochastic dynamics of half-platinized Janus sphere dimers similar to those herein, finding that most conformations follow circular trajectories. Other studies have investigated interaction of pairs of individual Janus particles [24,27–33] but not the stabilization of active dimers. Interactions in a similar system of active cylindrical motors have also been considered recently [34,35].

We study the conformation, stabilization, and dynamics of dimers of Janus microswimmers driven by a catalytic reaction. As shown in Fig. 1 these dimers can exist in different conformations. We discuss the statistics of dimers in the *cis*- and *trans*-conformations as a function of fuel concentration. Section II describes a complete parametrization of all possible dimer conformations. Symmetry arguments and a "zeroth-order" dynamical model reduces the conformation space to a convenient subspace for analysis of our experimental data. In Sec. III we present the experimental observations on dimer conformation statistics as a function of fuel concentration. Section IV contains a discussion of the results. We find the rapid spinning combined with little translational motion is likely to account for the prominence of the *trans*-dimer conformation at higher concentrations, and, for the most part, dimers form with stable conformations already before exposure to fuel.

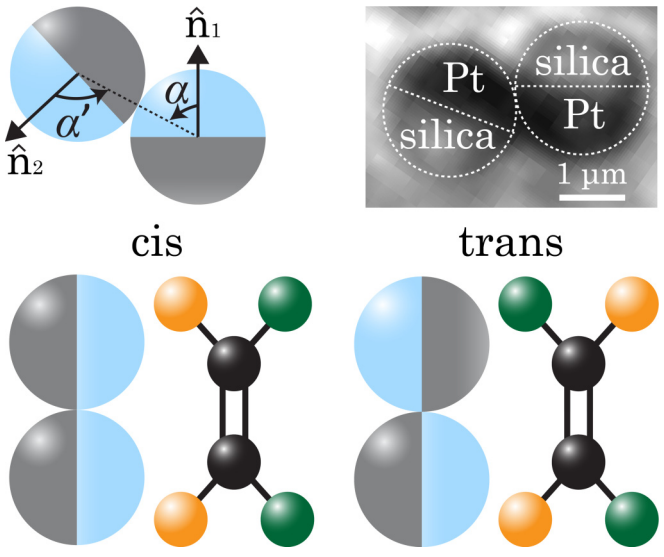

FIG. 1. Top left: the conformation of a dimer is characterized by a pair of angles (α,α'). Top right: an example video frame of a single dimer; the dark section shows the location of the platinum (Pt) and the rest of the particle is silica. Bottom: in analogy with cis-trans isomers of alkenes, the *cis*-conformation $(\frac{\pi}{2},-\frac{\pi}{2})$ has a plane of symmetry and moves rectilinearly while the *trans*-conformation $(\frac{\pi}{2},\frac{\pi}{2})$ rotates in-place.

*nourhani@psu.edu
†john.gibbs@nau.edu

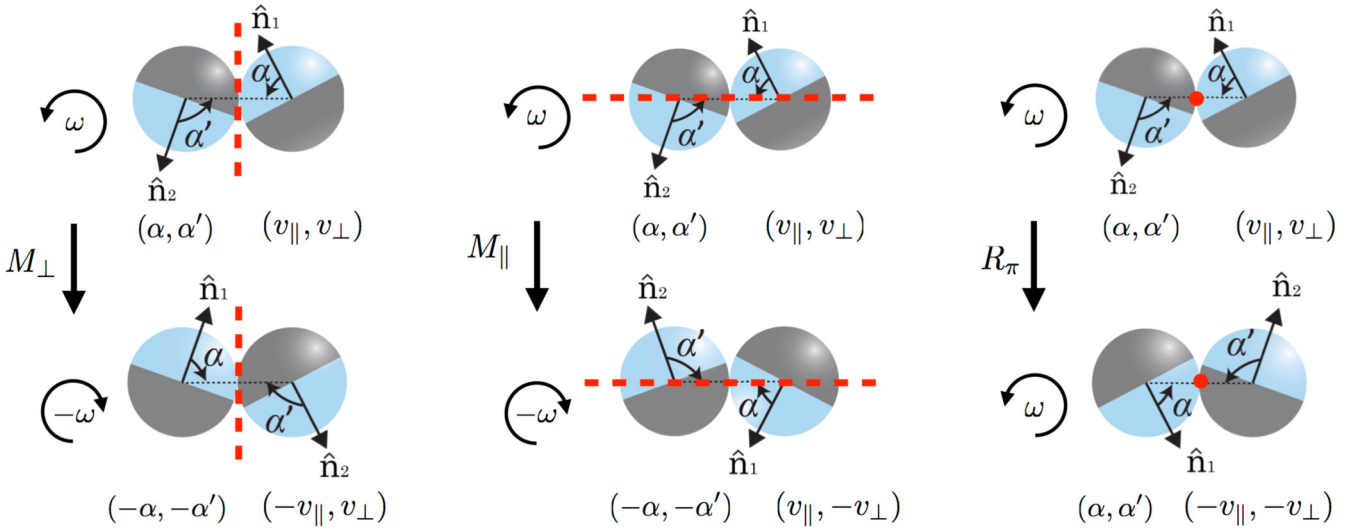

FIG. 2. Symmetry operations of Janus sphere dimers and their effects on conformation and dynamical characteristics. (Left) Reflection $M_\perp$ through the vertical plane tangent to both spheres at the contact point, (middle) reflection $M_\parallel$ through the vertical plane containing both sphere centers and the contact point, and (right) 180° rotation R_π about the contact point.

II. DIMER CONFORMATIONS

The Janus spheres automatically orient with their equatorial planes containing the vertical. Also, since they are all in the same plane, when they dimerize, the line segment joining the centers is horizontal. Thus, as shown in Fig. 1, the internal conformation of a Janus sphere dimer is completely specified by the pair of signed angles (α,α') from the radii through the centers of the platinum caps to those through the contact point, with $-\pi \leqslant \alpha,\alpha' < \pi$ (the angle is reckoned positive if the contact point is counterclockwise from the cap center, but π and $-\pi$ are completely equivalent). To the extent that the spheres are symmetric and identical, the deterministic part of a dimer's dynamics should be uniquely dictated by the angles α and α'.

We focus not upon the dimers' dynamics as such, but rather on the stabilization of the dimers and the internal relative orientations of the Janus spheres, as reflected in conformational statistics over a range of fuel concentration. We find two conformations to be particularly prevalent, especially at higher fuel concentrations, which we designate by analogy to *cis*- and *trans*-isomers. Experimentally, conformations close to $\pm(\frac{\pi}{2},\frac{\pi}{2})$ are approximated as "*trans*-dimers," and those close to $\pm(\frac{\pi}{2},-\frac{\pi}{2})$ are considered to be "*cis*-dimers," as will be discussed in Sec. III. In *trans*-dimers the active sites are oriented roughly in opposite directions, while *cis*-dimers are characterized by the alignment of the two Janus particles, as shown in the bottom-right and bottom-left of Fig. 1, respectively. For both conformations, the contact point is near the equators of the particles.

A. Conformation symmetries

Symmetry considerations, which are entirely independent of dynamical details, play an important simplifying role in our investigation. For a specific dimer, we take some arbitrary convention about which sphere position is first and which is second, so that, for conformation (α,α'), angle α pertains to the first sphere. Then, as shown in the left of Fig. 2, reflection $M_\perp$ through the vertical plane tangent to both spheres at the contact point will interchange them, producing a pair $(-\alpha',-\alpha)$. If the original pair had translational velocity components $(v_\parallel,v_\perp)$ along the intercenter direction and perpendicular to it, respectively, then the reflection will change the sign of $v_\parallel$, but not that of $v_\perp$. Finally, if the original pair had angular velocity ω (positive means the dimer spins counterclockwise), then the result of reflection has angular velocity $-\omega$. Similar analyses for a reflection $M_\parallel$ through the vertical plane containing both sphere centers and the contact point, and for $M_\perp$ and $M_\parallel$'s combination, which is really just a 180° rotation R_π about the contact point, lead to the rest of Fig. 2. As an example of its use, the entry for $M_\perp$ shows that if $\alpha = -\alpha'$, then the reflected pair is indistinguishable from the original, so that $v_\parallel = 0$. Such a pair must have translational velocity purely perpendicular to the intercenter line, though it could be zero. In the absence of noise, all other conformations follow circular trajectories with differing radii.

B. Dynamical model

To these symmetry considerations, we add a zeroth approximation dynamical model, specified by the assumptions (1) every Janus sphere generates a total motive force ($\mathbf{F}$) of the same magnitude (F), directed away from the platinum cap; (2) the distribution of motive forces is rotationally symmetric with respect to the symmetry axis of the Janus sphere; and (3) the motive forces acting on a Janus sphere are unaffected by dimer formation. These assumptions are clearly simplistic, but should yield qualitatively correct results. Assumption 2 means that, for purposes of computing the motive torque about the contact point, the motive force may be taken to act at the particle center. The motive torque about the contact point on a dimer is then

$$\begin{aligned}\tau_{\text{motive}} &= rF(\sin\alpha + \sin\alpha') \\ &= 2rF\sin\left(\frac{\alpha+\alpha'}{2}\right)\cos\left(\frac{\alpha-\alpha'}{2}\right). \end{aligned} \quad (1)$$

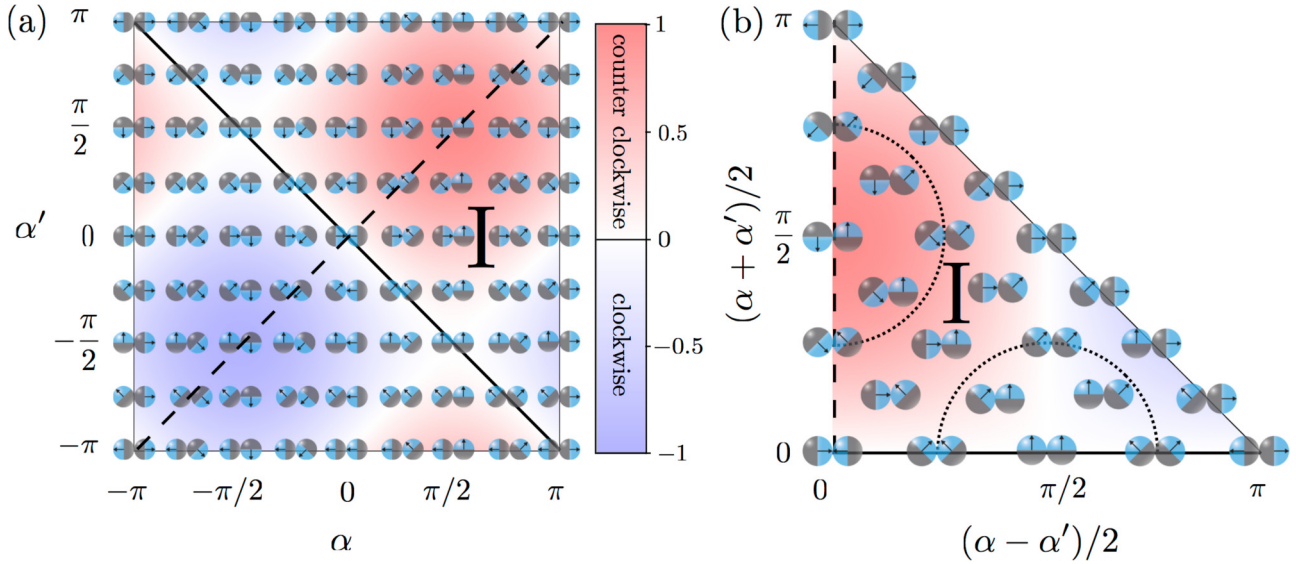

FIG. 3. (a) The density plot represents the intensity of the torque applied to the entire range of possible dimer conformations. The shaded regions show positive (counterclockwise - red) and negative (clockwise - purple) rotation primarily in the top right and bottom left regions of the density plot, respectively. Example dimer conformations are overlaid on the density plot. Physically, each of the four regions bordered by the diagonal lines (solid and dashed) contain identical dimers to each of the other three regions when only dynamics is considered (and chirality is disregarded). Thus, the dimers in the four regions can be mapped into a single triangular quadrant. We arbitrarily chose the quadrant marked as "I" for this mapping. (b) After mapping, the quadrant I is rotated by $\frac{\pi}{4}$ and the axes are adjusted to run from 0 to π. The dashed semicircles show the boundary for the region considered to be in the *trans*-conformation (top-left red region) and for the *cis*-conformation (bottom region) for the experimentally measured data points.

These particles operate in an overdamped Stokes flow regime. Therefore, the total torque on a dimer is zero, as the motive torque is countered by a viscous drag torque, $\tau_{\text{drag}} = -\tau_{\text{motive}}$; at low Reynolds number, that gives an angular velocity of the dimer proportional to the motive torque, i.e., $\omega \propto \tau_{\text{motive}}$. Figure 3(a) depicts the motive torque over the entire range of possible (α,α') pairs as a density plot, normalized by $2rF$, so that the maximum torque, attained by the counterclockwise spinning *trans*-dimer conformation takes value $+1.0$.

C. Reduction of the conformation space

The four quadrants of Fig. 3(a) are in a sense redundant. Reflection across the diagonal (dashed) line from $(-\pi,-\pi)$ to (π,π) corresponds to the operation R_π in Fig. 2. This operation interconverts conformations which are equivalent in a strong sense, as it is part of the normal time evolution. Reflection across the diagonal (solid) line from $(-\pi,\pi)$ to $(\pi,-\pi)$ reverses the sign of both conformation angles as well as the chirality, and corresponds to the operation $M_\parallel$. It thus connects conformations which are distinguishable in the ordinary course of things. However, unless the occurrence of one chirality has a higher frequency than the other, for the purpose of our study, nothing is lost by collapsing everything into a single quadrant with composite angles $(\alpha+\alpha')/2$ and $(\alpha-\alpha')/2$ as conformation parameters, using the group operations.

We arbitrarily choose the quadrant labeled "I", which is shown slightly expanded and conveniently rotated in Fig. 3(b). The crucial distinctions between *trans*-, *cis*-, back-to-back, front-to-front, and front-to-back conformations are now cleanly and uniquely represented. A conformation transformed into quadrant I is in normal form, which can also be characterized by $\alpha \geqslant |\alpha'|$.

III. EXPERIMENTAL RESULTS

A Janus microswimmer in our study is an isotropic silica sphere of 2 μm diameter with one hemisphere covered by a thin layer of platinum; we employed physical vapor deposition [36] to deposit platinum onto a monolayer of these spheres in a molecular beam epitaxy system. The Janus spheres self-propel in an aqueous solution of hydrogen peroxide due to the catalyzed reaction on the platinum surface [29,37–39]. We captured the particles' motions using bright-field video microscopy. Videos of the dimers in action can be found in the Supplemental Material [40].

Experimental dimer conformation data for a range of fuel concentrations are shown in Fig. 4(a), using the notation described in the previous section. Blue circles and green squares represent low concentrations of hydrogen peroxide, whereas red and yellow stars represent higher concentrations. Two trends are immediately apparent: (1) conformations are clustered near the *cis*- and *trans*-conformations, (2) with increasing fuel concentration, clustering around the *trans*-conformation becomes stronger, whereas the trend in clustering around the *cis*-conformation seems to be much weaker.

In order to quantify these observations, we distinguish a range of conformations as approximately *trans* or approximately *cis*. The corresponding regions on the plot are delimited by the dashed semicircles of radius $\pi/4$ centered on the ideal *trans*- and *cis*-conformations in Figs. 3(b) and 4(a). In formulas, the criteria are, approximately *trans* $= (\alpha-\pi/2)^2 + (\alpha'-\pi/2)^2 \leqslant (\pi/4)^2$, approximately *cis* $= (\alpha-\pi/2)^2 + (\alpha'+\pi/2)^2 \leqslant (\pi/4)^2$.

Figure 4(b) shows, as a function of hydrogen peroxide concentration, the percentage of approximately *trans*-dimers

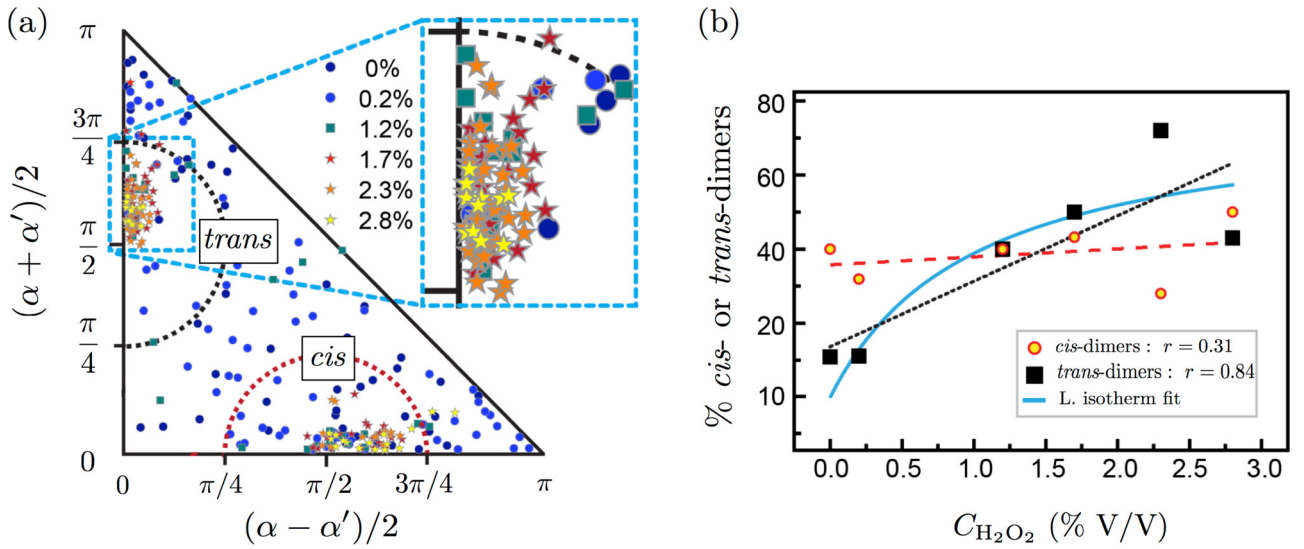

FIG. 4. (a) Data points for different concentrations of hydrogen peroxide $C_{H_2O_2}$ are color-coded the following way: blue and green circles and squares represent low concentrations and red and yellow stars represent higher concentrations. The dashed blue rectangular section is magnified to the right of the plot in order to better resolve the data points in that region, and the values of hydrogen peroxide concentration are to the left of the inset. The data points that fall within the semicircles are considered to be in the "experimentally" *trans*-conformation (top left) or *cis*-conformation (bottom center). (b) The data points show the percentage of dimers which were found to be in the *trans*-conformation (black squares) or the *cis*-conformation (yellow circles with red outline) as a function of hydrogen peroxide concentration. The red (dashed) and black (dotted) lines show the linear fit for the percentage of *cis*- and *trans*-dimers, respectively; the blue (solid) line shows a Langmuir fit to the *trans*-dimer data.

as black solid squares and the percentage of approximately *cis*-dimers as yellow circles with red outlines. The dotted black and dashed red lines are produced from (Levenberg-Marquardt algorithm) linear fits. A significant positive correlation between the proportion of *trans*-dimers and the hydrogen peroxide concentration is evident, while the correlation for *cis*-dimer proportion is much weaker. The Pearson product-moment correlation coefficients are $r = 0.84$, and $r = 0.31$, respectively. A fit to a Langmuir isotherm form $c/(a + c)$ is also shown as a solid blue curve in Fig. 4(b). We note that for the data points at 2.3% and 2.8%, the two dominant conformations add nearly to 100%.

IV. DISCUSSION

Consider now the conformation distribution in the absence of fuel. That corresponds to the dark blue dots in Fig. 4(a), but the more plentiful light blue dots are data for a very low concentration which probably shows no significant dynamical effects. Upon casual inspection, those data appear relatively uniformly spread, though with perhaps a little concentration in the acute corners. In the absence of fuel, dimers are expected to be held together primarily by van der Waals interactions, although other electrostatic interactions may also play a role [41–44]. Since the Hamaker constant for Pt is larger than for silica, van der Waals interactions would prefer dimers with their Pt caps together, precisely the conformations corresponding to the acute corners in the diagram. This may explain the slight clustering there. If nonisotropic electrostatic interactions are significant, they would be between dipoles parallel to the symmetry axes of the particles, and therefore would favor *trans*-conformations. No evidence is seen for that. Since the approximately *trans* and *cis* regions each occupy 0.197 of the triangle area, if the distribution were uniform, the proportion of approximately *trans*- or *cis*-dimers would be 0.197 ± 0.05 (there were 55 dimers in the sample at $C_{H_2O_2} = 0$). The *trans* population is consistent with a uniform distribution of conformations. *Cis*-dimers, on the other hand, are in gross excess, as shown in Fig. 4(b), and that excess persists over the entire concentration range. Anisotropic interactions would not be expected to favor the *cis*-conformation. Fortunately, there is a very simple, plausible explanation: the ordering of the spheres, onto which the catalyst is deposited, is hexagonal close-packed. Should some of the platinum accidentally form a "bridge" between two spheres, they would become permanently bonded in a *cis*-conformation.

We next turn to the trend observed for the *trans*-dimers with respect to fuel concentration. Although it is unclear what the detailed mechanism is, we nevertheless give a brief qualitative discussion through three points of interest.

(i) It appears that the abundance of *trans*-dimers is not a result of spontaneous formation after activation, but rather the dimers form before the addition of fuel, i.e., in water only. To come to this conclusion, we observed the particle suspension in water only, then added hydrogen peroxide solution to the same sample while keeping track of the particles. We were thus able to determine if single active particles undergoing self-assembly was responsible for forming the dimers; a video of the addition of fuel to the sample can be found in the Supplemental Material [40].

We did observe some formation events after the addition of fuel as demonstrated in the frames of Fig. 5(a); however, these events were extremely rare, and individual particles usually did not form dimers spontaneously, as shown in Fig. 5(b).

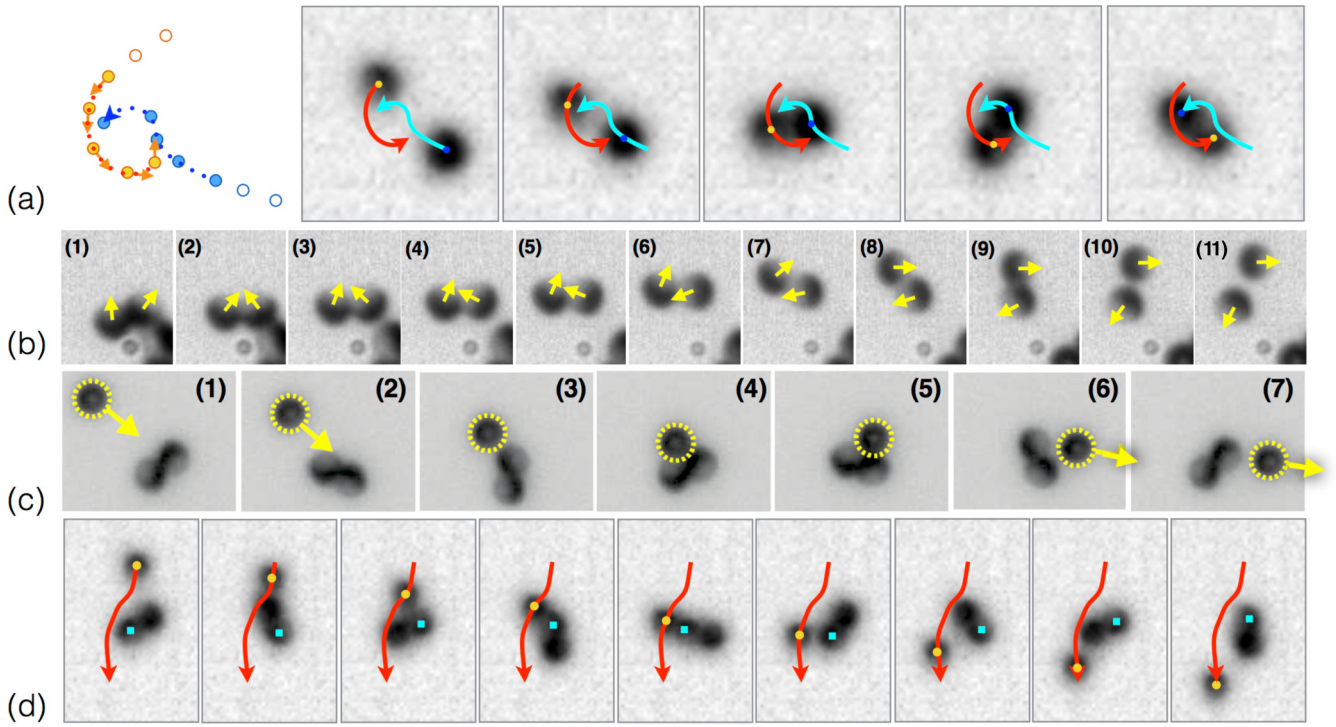

FIG. 5. (a) Interaction between two individual Janus spheres leads to a collapsing spiral ending in collision and dimer formation. (b) A dimer separates from an aggregate and the spheres slide over each other toward the *trans* conformation, but there does not seem to be rotation of the dimer as a whole as in (a), and the spheres eventually part ways. (c) A third particle fails to incorporate into a cluster for what appears to be a similar reason. The dimer is just spinning as it passes by. (d) A third particle (yellow dot) approaches a dimer, but is in an unfavorable position to be incorporated as it is pushed away by the particle marked by a blue square.

Furthermore, events of dimers *disassembling* into two single particles were never observed in any of our experiments, although larger clusters were observed splitting into smaller groups. It seems once a particle is locked in a dimer, it will remain there indefinitely, presumably stabilized by colloidal forces.

Additionally, we have no direct evidence of the relative angles changing with respect to time. This was inferred by observing the orbital behavior of the dimers after the addition of fuel. That is, the radius of their circular trajectory is expected to change if the angles fluctuated in time, but this was not observed. The above observations were general, and appeared to be true at all concentrations.

(ii) The circular orbits exhibited by dimers other than the *trans*-conformation were observed to assemble with larger clusters by what appears to be primarily "self-trapping," as seen in systems of single active Janus spheres [10]. The (ideal) *trans*-conformation remains roughly stationary (diffusion only) and spins in-place; thus it does not interact with other clusters as frequently as non-*trans*-conformations; the latter of which cover larger distances due to their orbital motion and thus have shorter average collision times.

(iii) At low concentration, even the *trans*-conformation is seen to self-assemble with larger clusters fairly readily, but, due to lower activity, interaction events are not as common as seen at high concentration. At the other end of the spectrum, at high concentration, it seems that the *trans*-dimers are impervious to forming larger aggregates, even though interaction events increase, in general, due to higher activity. Roughly, *trans*-dimers spin rapidly and are thus able to "kick" themselves away from larger clusters; further, we observed the *trans*-dimers ejecting approaching single particles attempting to form a larger cluster with the dimer. This effect is demonstrated in the video frames of Fig. 5(c). However, at low concentration, and thus low spinning frequency, the *trans*-dimers are not energetic enough for this effect to take place, allowing for merging with other clusters via short-range attractive forces.

Considering the above observations, the monotonic increase in the fraction of *trans*-dimers with concentration may be due to higher spinning frequency at higher concentrations, reducing the chance of self-assembly or being captured by another cluster; additionally, configurations other than the *trans*-dimer self-trap with larger clusters at a higher rate (than the *trans*-dimers), at all concentrations, because they are propelled translationally, and thus have a higher probability of becoming integrated with another cluster.

One last note concerning the *cis*-dimers: Should we see the percentage of this conformation decrease with increasing concentration since more interaction events are expected to lead to more clustering? Our data in Fig. 4 show that the percentage of *cis*-dimers slightly increases with concentration, seemingly contradicting this notion. However, this effect may also have a simple explanation: higher activity also means clusters are more likely to disassemble at steady state. For instance, single particles trapped in a cluster may escape by the metal cap reorienting to favor escape (propulsion direction being away from the cluster). Thus the *cis*-conformation may

be more likely to escape from a larger cluster since the propulsion of both Janus spheres is in the same direction, increasing the chance of escape.

As remarked earlier, formation events were rare, yet a few were observed and captured on video. A successful dimer formation event, as depicted in Fig. 5(a), depends on self-propulsion and short-range colloidal interactions, with phoretic and hydrodynamic interactions also likely involved. Vorticity in the flow generated by one particle appears to induce rotation in the second, as suggested by the curved arrows following the trajectories. This mutually induced rotation causes the particles to spiral toward one another, becoming locked by colloidal forces after contact. The longest-range influence, falling off as $1/r$ at large distance, is secondary to the motive mechanism, arising from the ordinary viscous drag on the self-propelled particles. Qualitatively, the effects are clear. Unless one is closest to a pole of the other, the spheres will tend to rotate away from each other if their velocity vectors form an acute angle, but toward each other if they form an obtuse angle. Thus, the spheres are more likely to come into close proximity if they are already in a roughly *trans* alignment. This may contribute to the increase in the proportion of *trans*-dimers with fuel concentration, though in view of the rarity of such events, it is a small effect. The dimer-formation failure depicted in Fig. 5(b) illustrates the dynamical delicacy. All appears to be going well until frame (9), where the direction of motion of the lower dimer seems to be just a bit too much away from the upper one.

Similar failures occur in building up larger clusters, as shown in Fig. 5(c). Here, it looks as though a third particle has been successfully integrated. Closer inspection reveals that the direction of motion of the third particle changes little during the encounter so that it easily slides off the dimer in panel (5). Figure 5(d) illustrates another failure mode, wherein the third particle is not in the right position and is pushed away by the rotating dimer.

In conclusion, we have considered the effect of fuel concentration, and therefore activity, on the stability of dimers made of active spherical Janus particles. We have discussed our observations that showed, at high activity, the *trans*-dimer conformation is dominant over all other conformations. We suggest this result is due to the combined effects of high rotation rate and little translational motion, enabling the *trans*-dimer to resist merging with a larger cluster.

ACKNOWLEDGMENTS

We thank the Peer Fischer group at the Max Planck Institute for Intelligent Systems, Stuttgart, Germany for providing the Janus particles. This project was funded by the State of Arizona Technology and Research Initiative Fund (TRIF), administered by the Arizona Board of Regents. A.N. and P.E.L. acknowledge funding by the National Science Foundation under Grant No. DMR-1420620 through the Penn State Center for Nanoscale Science.

[1] S. Sanchez, L. Soler, and J. Katuri, Angew. Chem., Int. Ed. **54**, 1414 (2015).
[2] F. Ginot, I. Theurkauff, D. Levis, C. Ybert, L. Bocquet, L. Berthier, and C. Cottin-Bizonne, Phys. Rev. X **5**, 011004 (2015).
[3] A. Nourhani and P. E. Lammert, Phys. Rev. Lett. **116**, 178302 (2016).
[4] L. C. Schmieding, E. Lauga, and T. D. Montenegro-Johnson, Phys. Rev. Fluids **2**, 034201 (2017).
[5] E. Mani and H. Löwen, Phys. Rev. E **92**, 032301 (2015).
[6] B. Liebchen, D. Marenduzzo, I. Pagonabarraga, and M. E. Cates, Phys. Rev. Lett. **115**, 258301 (2015).
[7] J. Bialké, T. Speck, and H. Löwen, J. Non-Cryst. Solids **407**, 367 (2015).
[8] J. Stenhammar, A. Tiribocchi, R. J. Allen, D. Marenduzzo, and M. E. Cates, Phys. Rev. Lett. **111**, 145702 (2013).
[9] G. S. Redner, M. F. Hagan, and A. Baskaran, Phys. Rev. Lett. **110**, 055701 (2013).
[10] I. Buttinoni, J. Bialké, F. Kümmel, H. Löwen, C. Bechinger, and T. Speck, Phys. Rev. Lett. **110**, 238301 (2013).
[11] A. Nourhani, P. E. Lammert, A. Borhan, and V. H. Crespi, Phys. Rev. E **87**, 050301 (2013).
[12] A. Nourhani, S. J. Ebbens, J. G. Gibbs, and P. E. Lammert, Phys. Rev. E **94**, 030601(R) (2016).
[13] F. Kummel, B. ten Hagen, R. Wittkowski, I. Buttinoni, R. Eichhorn, G. Volpe, H. Lowen, and C. Bechinger, Phys. Rev. Lett. **110**, 198302 (2013).
[14] H. Löwen, Eur. Phys. J.: Spec. Top. **225**, 2319 (2016).
[15] J. Gibbs and P. Fischer, Chem. Commun. **51**, 4192 (2015).
[16] J. Simmchen, J. Katuri, W. E. Uspal, M. N. Popescu, M. Tasinkevych, and S. Sánchez, Nat. Commun. **7**, 10598 (2016).
[17] M. Ibele, T. E. Mallouk, and A. Sen, Angew. Chem., Int. Ed. **48**, 3308 (2009).
[18] W. Wang, W. Duan, S. Ahmed, A. Sen, and T. E. Mallouk, Acc. Chem. Res. **48**, 1938 (2015).
[19] J. Schwarz-Linek, J. Arlt, A. Jepson, A. Dawson, T. Vissers, D. Miroli, T. Pilizota, V. A. Martinez, and W. C. Poon, Colloids Surf., B **137**, 2 (2016).
[20] M. Xuan, J. Shao, X. Lin, L. Dai, and Q. He, ChemPhysChem **15**, 2255 (2014).
[21] W. Wang, W. Duan, S. Ahmed, T. E. Mallouk, and A. Sen, Nano Today **8**, 531 (2013).
[22] A. Nourhani, V. H. Crespi, and P. E. Lammert, Phys. Rev. E **91**, 062303 (2015).
[23] A. Nourhani, P. E. Lammert, V. H. Crespi, and A. Borhan, Phys. Fluids **27**, 012001 (2015).
[24] W. Gao, A. Pei, X. Feng, C. Hennessy, and J. Wang, J. Am. Chem. Soc. **135**, 998 (2013).
[25] S. Ebbens, R. A. L. Jones, A. J. Ryan, R. Golestanian, and J. R. Howse, Phys. Rev. E **82**, 015304(R) (2010).
[26] I. Theurkauff, C. Cottin-Bizonne, J. Palacci, C. Ybert, and L. Bocquet, Phys. Rev. Lett. **108**, 268303 (2012).
[27] A. Wittmeier, A. Leeth Holterhoff, J. Johnson, and J. G. Gibbs, Langmuir **31**, 10402 (2015).
[28] N. Sharifi-Mood, A. Mozaffari, and U. Córdova-Figueroa, J. Fluid Mech. **798**, 910 (2016).
[29] L. Baraban, M. Tasinkevych, M. Popescu, S. Sanchez, S. Dietrich, and O. Schmidt, Soft Matter **8**, 48 (2012).

[30] H.-R. Jiang, N. Yoshinaga, and M. Sano, Phys. Rev. Lett. **105**, 268302 (2010).
[31] S. K. Smoukov, S. Gangwal, M. Marquez, and O. D. Velev, Soft Matter **5**, 1285 (2009).
[32] J. Yan, M. Han, J. Zhang, C. Xu, E. Luijten, and S. Granick, Nat. Mater. **15**, 1095 (2016).
[33] P. Bayati and A. Najafi, J. Chem. Phys. **144**, 134901 (2016).
[34] W. Wang, W. Duan, A. Sen, and T. E. Mallouk, Proc. Natl. Acad. Sci. U.S.A. **110**, 17744 (2013).
[35] M. S. D. Wykes, J. Palacci, T. Adachi, L. Ristroph, X. Zhong, M. D. Ward, J. Zhang, and M. J. Shelley, Soft Matter **12**, 4584 (2016).
[36] U. Choudhury, L. Soler, J. G. Gibbs, S. Sanchez, and P. Fischer, Chem. Commun. **51**, 8660 (2015).
[37] J. Palacci, C. Cottin-Bizonne, C. Ybert, and L. Bocquet, Phys. Rev. Lett. **105**, 088304 (2010).
[38] S. H. Klapp, Curr. Opin. Colloid Interface Sci. **21**, 76 (2016).
[39] J. Elgeti, R. G. Winkler, and G. Gompper, Rep. Prog. Phys. **78**, 056601 (2015).
[40] See Supplemental Material at http://link.aps.org/supplemental/10.1103/PhysRevE.95.042609 for videos of the dimers in action.
[41] A. Walther and A. H. Müller, Chem. Rev. **113**, 5194 (2013).
[42] J. Drelich and Y. U. Wang, Adv. Colloid Interface Sci. **165**, 91 (2011).
[43] S. Jiang, Q. Chen, M. Tripathy, E. Luijten, K. S. Schweizer, and S. Granick, Adv. Mater. **22**, 1060 (2010).
[44] S. C. Glotzer and M. J. Solomon, Nat. Mater. **6**, 557 (2007).